Journal of Alloys and Compounds 696 (2017) 234–238

Contents lists available at ScienceDirect

Journal of Alloys and Compounds

journal homepage: http://www.elsevier.com/locate/jalcom

Resistivity dependence of the spin mixing conductance and the anisotropic magnetoresistance in permalloy

Wenxu Zhang*, Ting Wu, Bin Peng, Wanli Zhang

State Key Laboratory of Electronic Thin Films and Integrated Devices, University of Electronic Science and Technology of China, Chengdu, 610054, PR China

ARTICLE INFO

Article history:
Received 21 July 2016
Received in revised form
10 October 2016
Accepted 19 November 2016
Available online 22 November 2016

Keywords:
Inverse spin Hall effects
Spin mixing conductance
AMR
Resistivity

ABSTRACT

Microwave spin pumping at ferromagnetic resonance from ferromagnetic films into nonmagnetic films is an efficient method to realize spin injection. The spin injection efficiency is proportional to the spin mixing conductance and can be detected by measuring voltages converted from spin current via the inverse spin Hall effect. In this work, we modified the properties of the ferromagnetic layer by thermal annealing. The results show that the crystal quality of the ferromagnetic films, as well as the magnetic properties has been greatly modified while the spin mixing conductance is insensitive to it. The work represent an incentive to work on engineering the spin Hall angle of the nonmagnetic layer to improve the spin Hall effect or the inverse spin Hall effect.

1. Introduction

There are several ways to inject spin currents from magnetically ordered materials to nonmagnetic materials by using polarized light, electron tunneling effects as well as heat gradient, etc. A recent review of these topics can be found in Refs. [1–3] and works cited therein. It was recently proposed that the spin can be pumped by microwave irradiation from the ferromagnetic (FM) materials to adjacent nonmagnetic (NM) metal materials [4,5]. This is an important breakthrough in this field, because the spins can be effectively injected from FM to NM metals in this way. DC voltages were generated in the NM metal due to the inverse spin Hall effect (ISHE), which follows the line shape of the ferromagnetic resonance (FMR) spectra. The spin current is converted to the charge current via the ISHE due to the spin-dependent scattering. Soon after, it was realized that in FM/NM bilayers, voltages at FMR have contributions not only from the ISHE, but also from the spin rectification effect (SRE) [6]. The SRE, according to the generalized Ohm's law, originates from the AMR effects, anomalous Hall effect and the phase differences between the RF magnetization and its current. The voltages are determined by three main processes: The magnetic moment is driven to process around certain effective field (H) by the microwave field. When the frequency (f_r) of the microwave magnetic field satisfies the condition that $f_r = \gamma H$, where γ is the gyromagnetic factor, FMR is achieved. The spin is generated (pumped out) from the ferromagnetic materials. Within the linear regime, the pumped spin current is proportional to the power of the microwave (P). The spins then diffuse through the interface, i.e. from FM to adjacent NM materials, which is characterized by a phenomenological parameter g_{mix} with $j_s = \frac{g_{mix}}{2\pi} P$. The diffused spin current (j_s) is then converted to electronic current (j_c) and the efficiency is expressed $\vec{j}_c = \frac{2e}{\hbar}\theta_{SH}\vec{j}_s \times \vec{\sigma}$, where θ_{SH} is the spin Hall angle, $\hbar$ is the Planck constant and e is the electron charge.

Annealing is a widely used technique to reduce defects and improve the crystalline in materials. In permalloy (Py, $Ni_{80}Fe_{20}$), annealing was report to be crucial to improve the anisotropic magnetoresistance (AMR) effect [7,8]. It was found that proper thermal treatment of the sample can release stress, promote crystal growth and reduce defects in the films [9,10]. It will also play its role in the SRE by changing the AMR effects. However, its influence to the spin-current conversion efficiency and, therefore, to the inverse spin Hall effects was less well studied. The process is sensitively dependent on the FM/NM interfaces, and crystalline quality of NM and FM layers. In this work, we perform a combination study of AMR effect, SRE and ISHE in Ta/Py/SiO_2(substrate) double layers with samples under different heat treatment. The results show that the heat treatment will influence the film magnetic performances, while the conversion efficiency of the microwave energy to electric voltages is insensitive to it within the accuracy of the present

* Corresponding author.
E-mail address: xwzhang@uestc.edu.cn (W. Zhang).

http://dx.doi.org/10.1016/j.jallcom.2016.11.274
0925-8388/

measurements.

2. Experimental details

The films were deposited by RF magnetron sputtering vacuum coating system at room temperature on SiO_2/Si substrates with dimensions of 5 × 10 × 0.5 mm [3]. The base pressure is 4.5×10^{-5} Pa and the working gas is Ar with purity of 5 N kept at 0.2 Pa. The target Py and Ta purity is 4 N and the film deposition rates are 6 nm/min and 12 nm/min, respectively. Seven NiFe (20 nm)/Ta (10 nm) and NiFe (20 nm) samples were prepared. After deposition, the annealing was carried out in-situ from 100 °C to 400 °C for 3.5 h.

The AMR is measured by the standard four-probe methods with source meter (KEITHLEY 2400). The magnetic field is applied in the film plane parallel and perpendicular to the long edge of the samples. The microwave related property measurement was performed by our shorted microstrip fixture which can work up to 8 GHz. We obtained the photonic voltage by lock-in techniques (SR830, Standford Research System) with microwave source provided by Rohde & Schwarz (SMB 100 A). At certain fixed microwave frequency, we swept the static magnetic field so that FMR was achieved. Separation of the SRE and ISHE signals was performed by the methods proposed by Zhang et al. [11] In order to put the samples at the same positions in the fixture and minimize the differences of the microwave field before and after sample flipping during measurements, we covered the samples with SiO_2/Si substrate of the same dimensions as the substrate.

3. Results and discussions

3.1. The AMR effect after annealing

The AMR of the Py monolayer and Py/Ta layer after annealing are shown in Fig. 1. In the bilayers, annealing gradually improves the AMR ratios from 0.5 to 1.0. Not only the absolute values of AMR is increased, but also the sensitivity of the AMR to the magnetic field is increased. It can be seen from the narrowed curves and reduced the full width at half maximum of the curves from 6 Oe to 4 Oe, which is because of the reduced coercivity of the films under annealing. The AMR in monolayer is higher than the double layers when annealed at the same temperature due to the shunt effect of the conducting Ta layer in the bilayers. The sheet resistance of Ta is about 68 $\Omega/_{\square}$, which is stable on annealing at the temperatures we used. Annealing reduces the resistivity of the films with only moderately improved ΔR. This can be confirmed by plotting the AMR with respect to resistivity ρ as shown in Fig. 2, where AMR is the ratio of ΔR to R. The reduction of the resistivity of NiFe film with the increase of the annealing temperature can be understood by increment of the grain size, and thus the grain boundary scattering can be reduced [10,12,13].

3.2. The magnetic parameters from SRE measurements

Typical photonic voltages obtained in Py and Py/Ta films are shown in Fig. 3. In Py monolayer, we have a combination of symmetric (V_L) and antisymmetric (V_D) Lorentzian contributions to the total voltage due to the SRE effects (seeing Fig. 3 (a)). As developed by Hu et al., [6] the SRE is another way to characterize magnetic films under microwaves magnetic field. In Ta/Py bilayers, the photonic voltage has additional contributions from ISHE due to the spins diffused into the Ta layer. The ISHE and SRE signals can be well separated by taking into account the symmetry of the two effects as shown in our previous work [11]. The voltages measured before and after sample flipping are shown in Fig. 3(b), together with the

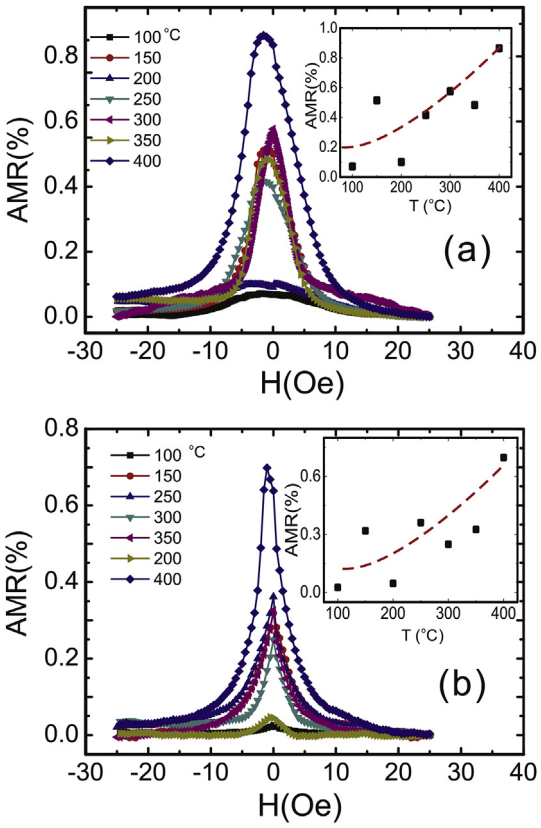

Fig. 1. AMR of samples annealed at temperatures from 100 °C upto 400 °C: (a) NiFe and (b) NiFe/Ta. The insets are the AMR vs. annealing temperatures with dashed curves to guide eyes. For clearness of the figure, only the values from $+H$ to $-H$ are shown. The data from $-H$ to $+H$ can be well reproduced by mirroring the data with respect to $H = 0$.

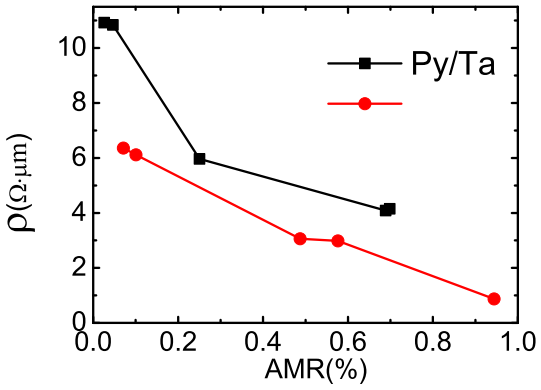

Fig. 2. AMR vs. resistivity of samples annealed at temperatures from 100 °C upto 400 °C.

separated contributions of SRE and ISHE curves.

From the SRE curve peaks, the resonance magnetic field (H_r) at the different resonant frequency (f) can be obtained in the samples. The H_r increases with the applied microwave frequencies as plotted in Fig. 4, which can be fitted to the Kittel's formula

$$f_r = \frac{\gamma}{2\pi}\sqrt{(H_r + H_k)\left(H_r + H_k + 4\pi M_{eff}\right)}, \quad (1)$$

where $4\pi M_{eff}$ is the effective saturation magnetization and H_k is

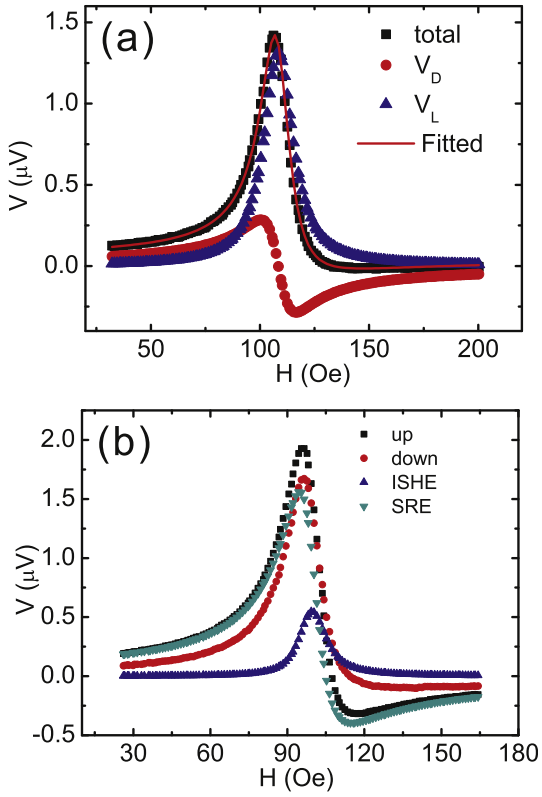

Fig. 3. Typical measured photonic voltage (V) as a function of applied field (H): (a) NiFe and (b)NiFe/Ta. The samples were annealed at 400 °C and measured at 3 GHz.

magnetocrystalline anisotropic constant. The fitting parameters are tabled and inset in the figure. The negative H_k means that the magnetic easy axis is perpendicular to the applied field which is along the long side of the film with our set-ups. The curves are generally divided into two groups as can be seen in the figures. The different groups have different magnetic properties, especially the saturation magnetization. We notice that the M_{eff} of the samples with ultra low AMR is also abnormally low, which is only about half of the other groups. This may be due to the poor crystallization of the NiFe film. However, the FMR absorption can still be well characterized in these films during our measurement. As shown in the table inset in the figures, the effective saturation magnetization is modified by annealing. It generally increases with the increment of the annealing temperatures, but the effect is not so controllable when the annealing temperature is low. We deduced that it is because the initial crystallization of NiFe shows certain randomness at low temperatures. At higher temperatures, the crystalline is much controlled.

Another important parameter obtained by FMR measurement is the FMR linewidth (ΔH). It is contributed from magnetic inhomogeneity induced frequency independent term ΔH_{inhom} and dissipation induced term ΔH_{hom} which is linearly dependent on the MW frequency (f).

$$\Delta H(f) = \Delta H_{inhom} + \Delta H_{hom}(f) \tag{2}$$

The Landau-Lifshitz (LL) damping parameter G is assumed to be an absolute constant, although spin-orbit coupling is generally believed to violate this assumption.

The measured curves of the samples are shown in Fig. 5(a) and (b). The films with low M_{eff} almost doubles the ΔH at the same

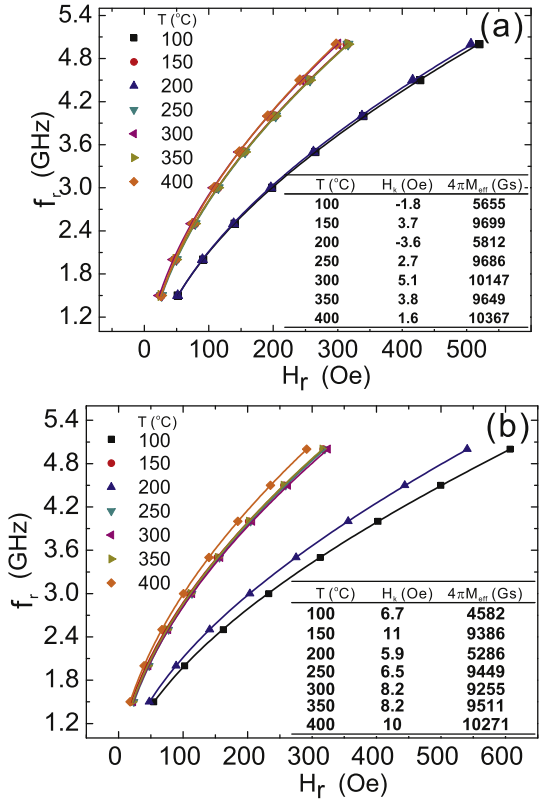

Fig. 4. Resonant frequency (f_r) as a function of applied field (H): (a) NiFe and (b)NiFe/Ta. Tables inset are the parameters obtained by fitting the curves to the Kittel's formula= $\Delta H_{inhom} + \frac{4\pi G}{\gamma^2 M_s} f$.

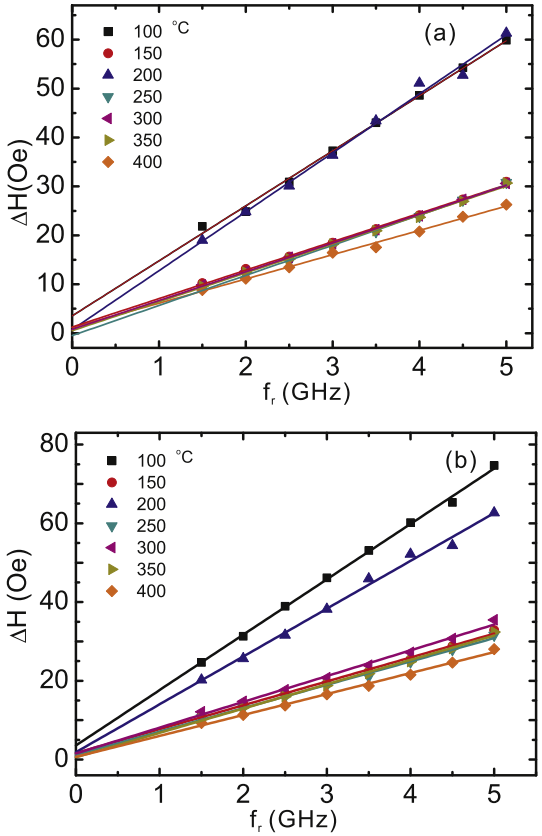

Fig. 5. FMR linewidth vs. resonant frequency (f_r) for NiFe monolayer (a) and NiFe/Ta bilayer (b).

frequency. This is mainly caused by the reduced M_{eff} as can be observed in Equ. (2). When compared the slope of the lines, we can see the increment of the slope when the Py films were covered with Ta. This enhancement of damping is due to the diffusion of the spins from FM to NM as generally accepted. This concept will be used to determine the spin mixing conductance as discussed below.

Extrapolation of the lines to $f = 0$ GHz gives ΔH_{inhom} less than 5 Oe in both monolayer and bilayers, indicating that the film inhomogeneity is small. This means that Py and Py/Ta films are of the same quality. Covering Py with Ta does not improve the film crystallization while a Ta layer underneath is frequently used to improve crystalline as a buffer layer. Relating the dimensionless Gilbert damping α to the LL parameter by $\alpha = G/\gamma M_s$, and plotted with respect to the resistivity (ρ) of Py, we find that both samples show increment of α with ρ as shown in Fig. 6. It confirms that electron scattering is one of the main sources of linewidth broadening as discussed by Ingvarsson et al. [14] The electron scattering time is proportional to the spin relaxation time in this diffusion regime.

3.3. The spin mixing conductance

The diffusion of spins from the FM layer to the NM layer generates charge current via the ISHE. In these experiments, the spin mixing conductance g_{mix} is the parameter which reflects the probability of the transferred spin moment and losses of the spin angular moment. It is the source of the FMR linewidth broadening, The spin mixing conductance enters the ISHE voltage, as derived by Mosendz et al. [15],

$$V_{ISHE} = \frac{-e\theta_{SH} g_{mix}^{eff} \lambda_s \tanh\left(\frac{t_N}{2\lambda_s}\right)}{t_N/\rho_N + t_F/\rho_F} LEf \sin^2\Theta, \quad (3)$$

where L, E, and λ_s correspond to the length of the bilayer, a correction factor for the ellipticity of the magnetization precession, and the spin diffusion length in the normal metal, respectively. $t_N/\rho_N + t_F/\rho_F = \frac{L}{Rw}$ where $\rho_{N(F)}$ and $t_{N(F)}$ are the resistivity and thickness of the nonmagnetic (ferromagnetic) layers with width being w. The dynamic magnetization ellipticity $E = \frac{2\omega_f[\omega_M + \sqrt{\omega_M^2 + 4\omega_f^2}]}{\omega_M^2 + 4\omega_f^2}$, with $\omega_M = \gamma 4\pi M_{eff}$ and $\omega_f = 2\pi f$, respectively. For our samples, we estimate the $E \sim 1.1$. At ferromagnetic resonance, the magnetization precession cone angle $\Theta = 2h_{rf}/\Delta H$, with the microwave magnetic field $h_{rf} \sim 0.1$ Oe as determined by

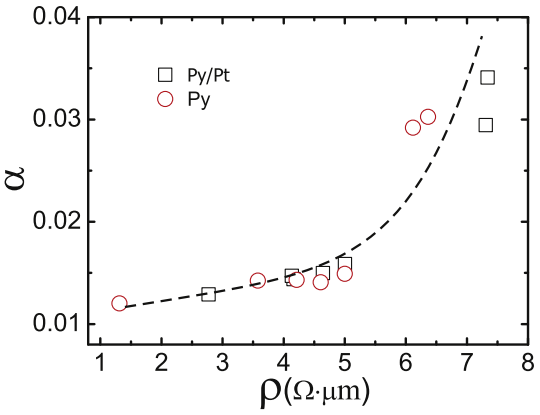

Fig. 6. Correlation between the Gilbert damping constant α and Py film resistivity ρ. For the bilayers, the resistance of Ta is subtracted. The squares and circles are from Py/Pt and Py respectively. The dashed line is for guiding eyes.

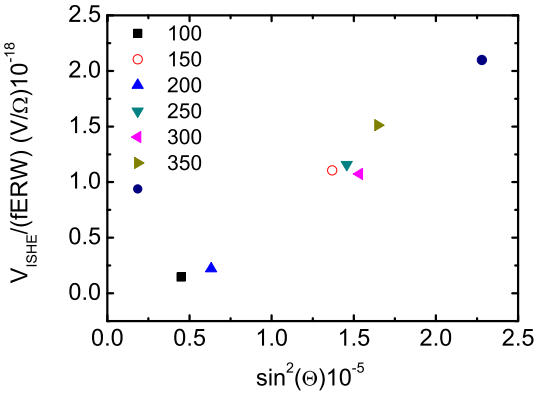

Fig. 7. The dc voltage V_{ISHE} induced by FMR scales with $\sin^2(\Theta)$ from samples with different annealing temperatures. The dashed line is for guiding eyes.

the measurement of the additional magnetic losses at FMR with and without samples [16]. Because the bilayer samples are different only in the FM layer, we can ascribe the same Ta related parameters in the measurement. Rearrangement of Equ. (3) gives

$$\frac{V_{ISHE}}{fERw} = -eCg_{mix}^{eff} \sin^2(\Theta), \quad (4)$$

where C contains all the parameters determined from NM layer. In this way we can plotted the $V_{ISHE}/(fERw)$ versus $\sin^2(\Theta)$ as shown in Fig. 7. The products of the two undetermined parameters θ_{SH} and g_{mix}^{eff} can be extracted from the slope of the lines.

As can be seen in the figure, the different samples shows only slightly different slopes, indicating that the products Cg_{mix}^{eff} is determined mainly by the nonmagnetic layer as predicted by the scaling relation from Equ. (4).

The conventional method to calculate the spin mixing conductance is calculated by comparison of the $\Delta H \sim f$ line slopes, as depicted in Fig. 5 from samples with and without NM layers as

$$\Delta H_{Py/Ta} - \Delta H_{Py} = g_{mix}^{tot} \frac{g\mu_B f}{2\gamma M_{eff} t_f}. \quad (5)$$

The increase of the line width determines the total loss of the spin angular moment. We plotted the spin mixing conductance g_{mix}^{tot} and g_{mix}^{eff} obtained from the above methods against the resistivity of the samples as shown in Fig. 8. If we compare the data from the

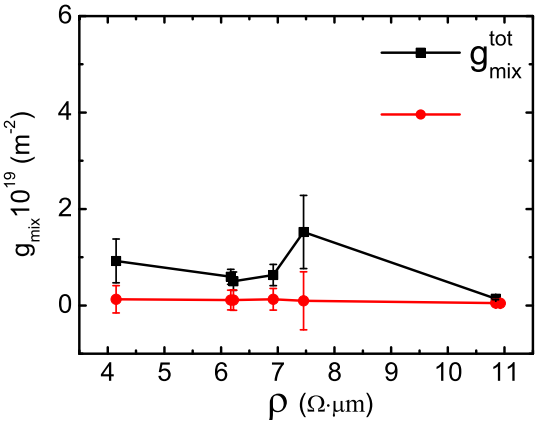

Fig. 8. The spin mixing conductance g_{mix} versus the resistivity ρ of the samples.

different methods, they are at the same scale and comparable with data obtained from other independent works. The agreement between the data from the different evaluation methods indicates that the loss of spin momenta is converted to the voltage via the inverse spin Hall effect in this conductive materials. The scaling behavior is in agreement with previous investigations [17,18]. Despite the agreement we obtained within the accuracy of the our present measurements, our work is incentive to further theoretical and experimental work to investigate the influence of FM layer to the spin mixing conductance. As the theoretical work shows that the spin polarization should play its role in the spin mixing conductance [19]. Insertion of Cu layer can increase the spin mixing conductance in Py/Ta, while it is decreased in Py/Pt as shown in experiments [20]. Based on the work up to now, we can only conclude that how is the different interface influence this parameter is still an open question.

4. Conclusions

In this work, we have fabricated Py monolayer and Py/Ta bilayers and then annealed them in vacuum up to 400 °C. ISHE and SRE voltages where measured under FMR. Annealing is an effective way to reduce the resistivity of the Py layer and enhance the AMR effect. However, it has only marginal influences on spin diffusion. At the same times, the spin mixing conductance is not scaled with the resistivity of the FM layer. In this case, the photonic voltages should be mainly dominated by the spin Hall angle which deserves materials engineering.

Acknowledgements

Financial supports from NSFC (61471095), “863”-projects (2015AA03130102) and Research Grant of Chinese Central Universities (ZYGX2013Z001) are acknowledged.

References

[1] A. Hoffmann, IEEE Trans. Mag. 49 (2013) 5172.
[2] A. Hoffmann, S.D. Bader, Phys. Rev. Appl. 4 (2015) 047001.
[3] J. Wunderlich, C.H. Back, T. Jungwirth, J. Sinova, S.O. Vanlenzuela, Rev. Mod. Phys. 87 (2015) 1213.
[4] J. Ieda, H. Kurebayashi, T. Trypiniotis, C.H.W. Barnes, S. Maekawa, E. Saitoh, K. Ando, S. Takahashi, Nat. Mater. 10 (2011) 655.
[5] H. Kurebayashi, O. Dzyapko, V.E. Demidov, D. Fang, A.J. Ferguson, S.O. Demokritov, Appl. Phys. Lett. 99 (2011) 162502.
[6] Y.S. Gui, X.L. Fan, M. Harder, Z.X. Cao, C.M. Hu, Phys. Rev. B 84 (2011) 054423.
[7] H. Funaki, S. Okamoto, O. Kitakami, Y. Shimada, Jpn. J. Appl. Phys. 33 (1994) L1304.
[8] M.F. Toney, W.Y. Lee, D. Mauri, IEEE Trans. Mag. 36 (2000) 381.
[9] A. Siritaratiwat, E.W. Hill, J. Mag. Mag. Mat. 198 (1999) 85.
[10] S. Krongelb, A. Gangulee, G. Das, IEEE Trans. Mag. 9 (1973) 568.
[11] W.X. Zhang, B. Peng, F.B. Han, Q.R. Wang, W.T. Soh, C.K. Ong, W.L. Zhang, Appl. Phys. Lett. 108 (2016) 102405.
[12] C.J. Zhao, L. Ding, J.S. HuangFu, J.Y. Zhang, G.H. Yu, Rare Met. 32 (2013) 213.
[13] A. Göktaş, A. Tumbul, F. Aslan, J. Sol. Gel Sci. Technol. 78 (2016) 262.
[14] S. Ingvarsson, L. Ritchie, X.Y. Liu, G. Xiao, J.C. Slonczewski, P.L. Trouilloud, R.H. Koch, Phys. Rev. B 66 (2002) 214416.
[15] O. Mosendz, J.E. Pearson, F.Y. Fradin, G.E.W. Bauer, S.D. Bader, A. Hoffmann, Phys. Rev. Lett. 104 (2010) 046601.
[16] R. Iguchi, K. Ando, R. Takahashi, T. An, E. Saitoh, T. Sato, Jpn. J. Appl. Phys. 51 (2012) 103004.
[17] F.D. Czeschka, L. Dreher, M.S. Brandt, M. Weiler, M. Althammer, I.M. Imort, G. Reiss, A. Thomas, W. Schoch, W. Limmer, H. Huebl, R. Gross, S.T.B. Goennenwein, Phys. Rev. Lett. 107 (2011) 046601.
[18] M. Weiler, M. Althammer, M. Schreier, J. Lotze, M. Pernpeintner, S. Meyer, H. Huebl, R. Gross, A. Kamra, J. Xiao, Y.T. Chen, H. Jiao, G.E.W. Bauer, S.T.B. Goennenwein, Phys. Rev. Lett. 111 (2013) 176601.
[19] Y. Liu, Z. Yuan, R.J.H. Wesselink, A.A. Starikov, P.J. Kelly, Phys. Rev. Lett. 113 (2014) 207202.
[20] P. Deorani, H. Yang, Appl. Phys. Lett. 103 (2013) 232408.